

Cite this: *Nanoscale*, 2018, **10**, 9141

Mesoporous silica nanoparticles induced hepatotoxicity via NLRP3 inflammasome activation and caspase-1-dependent pyroptosis[†]

Xuyao Zhang, ^{‡a,b} Jingyun Luan, ^{‡a,b} Wei Chen, ^{a,b} Jiajun Fan, ^{a,b} Yanyang Nan, ^{a,b} Yichen Wang, ^{a,b} Yanxu Liang, ^{a,b} Guangxun Meng^c and Dianwen Ju ^{*,a,b}

Increased biomedical applications of mesoporous silica nanoparticles (MSNs) raise considerable attention concerning their toxicological effects; the toxicities of MSNs are still undefined and the underlying mechanisms are unknown. We conducted this study to determine the hepatotoxicity of continuous administration of MSNs and the potential mechanisms. MSNs caused cytotoxicity in hepatic L02 cells in a dose- and time-dependent manner. Then, MSNs were shown to elicit NOD-like receptor protein 3 (NLRP3) inflammasome activation in hepatocytes, leading to caspase-1-dependent pyroptosis, a novel manner of cell death. *In vivo* MSN administration triggered hepatotoxicity as indicated by increased histological injury, serum alanine aminotransferase and serum aspartate aminotransferase. Notably, NLRP3 inflammasome and pyroptosis were also activated during the treatment. Meanwhile, in NLRP3 knockout mice and caspase-1 knockout mice, MSN-induced liver inflammation and hepatotoxicity could be abolished. Furthermore, experiments indicated that MSNs induced mitochondrial reactive oxygen species (ROS) generation, and the ROS scavenger could attenuate the MSN-activated NLRP3 inflammasomes and pyroptosis in the liver. Collectively, these data suggested that MSNs triggered liver inflammation and hepatocyte pyroptosis through NLRP3 inflammasome activation, which was caused by MSN-induced ROS generation. Our study provided novel insights into the hepatotoxicity of MSNs and the underlying mechanisms, and facilitated the potential approach to increase the biosafety of MSNs.

Received 20th January 2018,
Accepted 5th April 2018

DOI: 10.1039/c8nr00554k
rsc.li/nanoscale

1. Introduction

The extensive applications of nanotechnology, especially nano-material-based drug delivery systems for imaging, diagnosis and therapy, have increased considerable concerns about the biosafety impacts caused by the engineered nanomaterials.^{1–3} Due to the attractive properties, including ingenious chemical modification, large pore volume and high specific surface area, mesoporous silica nanoparticles (MSNs) have been regarded as effective delivery systems for various therapeutic

approaches to treat against many types of diseases such as diabetes, malignancy and bone tissue engineering.^{4–6} So far, most of the toxicity studies of silica nanoparticles focus on the bio-behavior of nanoparticles that accidentally enter the body (mainly inhalation of nanomaterials).^{7,8} However, biological and biomedical applications of these silicon nanoparticles for diagnosis or theranostic agents require the administration routes such as intramuscular, subcutaneous or intravenous.^{9–11} *In vivo* experiments have shown that MSNs caused morphological and functional impairments in the liver.¹² Even so, the scientific basis for the toxicological effects of MSNs is poorly elucidated and the underlying mechanism is still finite, posing far-reaching challenges to their practical application.

The reticuloendothelial system including the liver, lymph nodes and spleen has been demonstrated to play crucial roles in nanoparticle recognition and clearance.^{13,14} Although strategies including PEGylation are conducted to help nanoparticles be hidden from the reticuloendothelial system, the liver is still recognized as one of the main targets of nanoparticles.¹⁵ Accumulating research studies have demonstrated that these nanoparticles may have hepatotoxicity when they

^aMinhang Hospital, Fudan University, 170 Xinsong Road, Shanghai 201199, China.
E-mail: dianwenju@fudan.edu.cn; Fax: +86 21 51980036; Tel: +86 21 51980037

^bDepartment of Microbiological and Biochemical Pharmacy & The Key Laboratory of Smart Drug Delivery, Ministry of Education, School of Pharmacy, Fudan University, Shanghai, 201203, China

^cUnit of Innate Immunity, Key Laboratory of Molecular Virology & Immunology, Institute Pasteur of Shanghai, Chinese Academy of Sciences, Shanghai, 200031, China

†Electronic supplementary information (ESI) available: Additional hematoxylin and eosin staining, immunoblotting analysis and confocal microscopy data. See DOI: 10.1039/c8nr00554k

‡These authors shared equal contribution.

directly enter the bloodstream, however the molecular mechanism is still unclear.^{12,16} Although the significance of MSNs is increasing in biomedical applications, limited studies have been conducted to examine the hepatotoxicity.¹⁶ Thus, full research on the hepatotoxicity of MSNs and especially the potential molecular mechanisms is needed.

NOD-like receptor protein 3 (NLRP3) inflammasome is an intracellular multiprotein complex based on a C-terminal leucine-rich domain, an N-terminal pyrin domain (PYD) and a nucleotide-binding domain.¹⁷ When NLRP3 inflammasome is triggered, the PYD recruits pro-caspase-1 and apoptotic speck-like protein to form a complex, resulting in the cleavage of caspase-1 and the maturation of interleukin-18 (IL-18) and interleukin-1 β (IL-1 β), which play a critical role in promoting liver inflammation.¹⁸⁻²⁰ Except for processing the proinflammatory cytokines, caspase-1 activation has been reported to induce a novel cell death form named pyroptosis, accompanied by DNA cleavage, cytoplasmic swelling, plasma membrane rupture and the release of the pro-inflammatory intracellular contents.²¹ In addition to the priming signal that activates NLRP3 by binding the toll-like receptor to lipopolysaccharide, other signals provided by activators are also needed, especially the cellular stress-released danger-associated molecular patterns, including excess adenosine triphosphate and cholesterol crystals, while mitochondria-derived reactive oxygen species (ROS) are considered as major activators.^{22,23} The abnormal NLRP3 always contributes to the progress of inflammatory diseases, including diabetes, Alzheimer's disease and atherosclerosis.^{24,25} To date, particulate irritants and nanoparticles, including alum, titanium dioxide (TiO_2), polyamidoamine (PAMAM) dendrimer, quantum dots (QDs) and silica dioxide, have been proved to induce NLRP3 inflammasome activation, resulting in inflammatory injury.²⁶⁻²⁹ However, as an extensively applied nanomaterial, whether the activation of NLRP3 inflammasomes

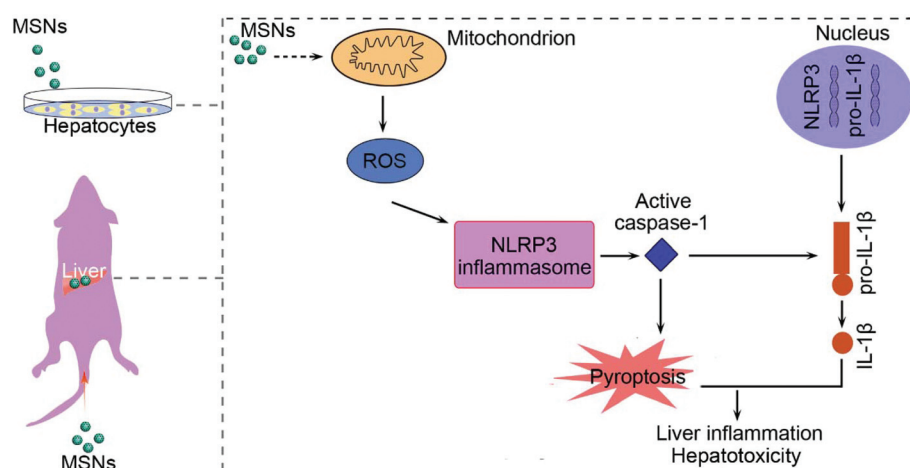
participates in the toxicity of MSNs and the precise mechanisms are poorly understood.

In this study, we investigated the role of NLRP3 inflammasome in MSN-mediated hepatotoxicity and showed that the administration of MSNs elicited NLRP3 inflammasome activation, leading to the inflammatory pyroptosis in hepatocytes and liver tissues (Scheme 1). Furthermore, MSN-induced liver inflammation could be abolished *via* depleting NLRP3 inflammasome in NLRP3 knockout ($NLRP3^{-/-}$) mice and caspase-1 knockout ($Caspase-1^{-/-}$) mice, demonstrating the crucial role of NLRP3 inflammasomes in MSN-elicited cytotoxicity. Importantly, our experiments indicated that MSNs induced mitochondria dysfunction and ROS production, and that the elimination of ROS attenuated the pyroptosis and NLRP3 inflammasomes elicited by MSNs.

2. Experimental

2.1. Preparation and characterization of MSNs

MSNs were synthesized as previously described.^{15,30} Briefly, the MSNs with generational and center-radial mesopore channels were achieved through a one-pot biphasic stratification approach as follows. Triethanolamine (TEA) and hexadecyltrimethylammonium bromide (CTAB) were added to water, then tetraethyl orthosilicate was added to the solution (water-CTAB-TEA) and kept under magnetic stirring. To obtain the products, the reaction mixture was then kept at 60 °C under continuous stirring for 12 h. The products were collected by centrifugation. Then residual reactants and surfactant templates were removed by ethanol and ammonium nitrate ethanol solution, respectively. A JEOL 2011F transmission electron microscope was employed to observe the morphology and structure of MSNs. Nanoparticle size and monodispersion of MSNs were determined by DLS (Malvern, UK) at 25 °C.



Scheme 1 Schematic diagram of MSN-induced hepatotoxicity and the underlying molecular mechanisms. MSNs induced ROS generation in hepatocytes, and then triggered NLRP3 inflammasome activation, leading to IL-1 β production and caspase-1-dependent pyroptosis, finally resulting in liver inflammation and hepatotoxicity.

2.2. Cell culture and treatment

L02 (human hepatic cell) was obtained from the Cell Bank of Shanghai Institutes for Biological Sciences, Chinese Academy of Sciences and cultured in RPMI 1640 medium, containing 10% FBS (Invitrogen, USA), 100 $\mu\text{g mL}^{-1}$ of streptomycin and 100 U mL^{-1} of penicillin (Beyotime Institute of Biotechnology, Hangzhou). After being primed with lipopolysaccharide (200 ng mL^{-1}) for 2 hours, hepatic cells were treated with MSNs under the indicated concentrations for 24 h and 48 h, respectively. Hepatic cells were pre-treated with MCC950 (NLRP3 inhibitor, 10 μM) and NAC (*N*-acetyl-L-cysteine, 5 mM) for 2 h, and then co-treated with MSNs.

2.3. *In vivo* experiments

All animal procedures were performed in accordance with the Institutional Guidelines for Care and Use of Laboratory Animals of Fudan University and approved by the Animal Ethics Committee of School of Pharmacy at Fudan University (agreement number 2017-03-WS-JDW-01). Six- to eight-week-old BALB/c mice were purchased from Shanghai SLAC Laboratory Animal Co. Ltd. NLRP3 knockdown mice (*NLRP3*^{-/-}) had been described before,^{31,32} and caspase-1 knockdown mice (*Caspase-1*^{-/-}) were obtained from Jackson Laboratory. Both *NLRP3*^{-/-} and *Caspase-1*^{-/-} mice had been crossed with BALB/c mice for 10 generations for the current project. Mice were intravenously injected with MSNs at a dose of 50 mg kg^{-1} three times a week. MCC950 and NAC were injected intraperitoneally at doses of 10 mg kg^{-1} day⁻¹ and 100 mg kg^{-1} day⁻¹, respectively. Three weeks later, liver tissues and the serum were collected for following experiments.

2.4. Cytotoxicity assay

Cell viability of hepatic cells was detected by the MTT assay. Hepatic cells were seeded into plates, followed by treatments with MSNs for the indicated time. Then the cells were cultured with MTT (0.5 mg mL^{-1}) for 4 h. Formazan crystals were dissolved with DMSO (100 μL each well). The optical density (O.D.) values at the wavelength of 570 nm were determined and cell viability was shown as the ratio of the O.D. values of MSN-treated cells relative to those of the control cells.

2.5 Release of LDH

After MSN treatment, CytoTox 96 Non-Radioactive Cytotoxicity Assay (Promega, USA) was used to measure the LDH level of the supernatants and the serum, respectively.³³ The O.D. value was read at 490 nm with a microplate reader and LDH release was expressed as the ratio of the value of the MSN-treated group relative to that of control.

2.6. siRNA transfection of NLRP3

Human *NLRP3* siRNA (siG12319173004) and the nonsilencing scrambled control (SCR) siRNA (siN058151221147) were purchased (Guangzhou RiboBio Co., Ltd, China). Following the manufacturer's instructions, hepatic cells were transfected

with siRNA using LipofectamineTM 2000 Transfection Reagent (Invitrogen, USA).

2.7. Flow cytometry assay

Pyroptosis was determined by using a FAM-FLICA Caspase-1 Detection kit (ImmunoChemistry, USA). Briefly, after treatment with MSNs and/or MCC950 and si-NLRP3 for 24 h, the samples were harvested to stain with FAM-YVAD-FMK green dye and PI red dye. Then a flow cytometer (BD FACSAria II, USA) was employed to analyze the samples, and PI red and FAM-YVAD-FMK green double stained cells were defined as pyroptosis.

2.8. Confocal microscopy

Unfixed frozen liver sections were harvested to detect pyroptosis, ROS and mitochondrial membrane potential. Briefly, a FAM-FLICA Caspase-1 Detection kit was employed to detect pyroptosis, and a MitoSoxTM red mitochondrial superoxide indicator and a mitochondrial membrane potential assay kit were purchased to examine mitochondrial ROS and mitochondrial membrane potential, respectively. The images were obtained according to the manufacturer's instructions of AttovisionTM software.

2.9. Immunoblotting analysis

Hepatocytes were subjected to total protein extraction and the extracted proteins were separated by SDS-PAGE and then transferred to PVDF membranes. Following the blockage of non-specific sites with bovine saline albumin (5%) and incubation with indicated primary antibodies, the PVDF membranes were subjected to HRP-conjugated secondary antibodies. The primary antibodies of anti-cleaved caspase-1, anti-NLRP3, anti-caspase-1, anti-IL-1 β and anti- β -actin were purchased from Cell Signaling Technology (Danvers, USA). The HRP-conjugated secondary antibodies were obtained from MR Biotech (Shanghai, China). ImmobilonTM Western Chemiluminescent HRP Substrate (Millipore, USA) was used to detect the immunoreactive bands. ImageJ software was employed to quantify the densitometric values of the resulting bands.

2.10. Immunofluorescence staining

The hepatocytes and liver sections were fixed in paraformaldehyde (4%) and permeabilized with Triton X-100 (0.2%) for ten minutes and then incubated with goat anti-NLRP3 antibody (Abcam, ab4207) for 2 h. Subsequently, the samples were incubated with donkey anti-goat IgG (Abcam, ab150131) and Hoechst33342 for 1 h. Confocal microscopy was used to observe and obtain the images.

2.11. Analysis of serum ALT and AST

A serum alanine aminotransferase (ALT) assay kit and a serum aspartate aminotransferase (AST) assay kit (Nanjing Jiancheng Bioengineering Institute, China) were purchased to examine the serum ALT and serum AST following the manufacturer's instructions.

2.12. Analysis of serum cytokines

Serum samples were collected from *NLRP3*^{-/-} mice, *Caspase-1*^{-/-} mice and WT mice to detect IL-1 β and IL-18 by using an enzyme-linked immunosorbent assay kit (ELISA kit, Multi Sciences, Hangzhou, China) following the manufacturer's instructions.

2.13. Caspase-1 activity measurements

The caspase-1 activity was measured by using a Caspase-1 Activity Assay kit (Beyotime Biotechnology, Haimen, China). Briefly, 50 μ g protein from liver homogenates was added to reaction buffer containing Ac-YVAD- ρ NA. The absorbance was read at 405 nm with a microplate reader and the caspase-1 activity was normalized for total proteins of cell lysates.

2.14. Statistical analysis

GraphPad Prism 5 (GraphPad Software Inc., USA) was used to analyze the data and the results were presented as mean \pm standard deviations (SD). Comparisons were performed by Student's *t* test or one-way ANOVA analysis. *P* value <0.05 was considered statistically significant.

3. Results

3.1. Characterization and hepatotoxicity of MSNs

The morphology and structure of the MSNs were observed with TEM, the average size and monodispersion of the MSNs were measured by using a Zetasizer and Fig. 1A shows that the mean diameter of MSNs was approximately 109.2 nm. The viability of hepatocytes under various concentrations of MSNs was analyzed by cytotoxicity assay and LDH release assay. After the hepatocytes were exposed to MSNs for 24 h or 48 h, a dose-dependent decrease of the cell viability was observed (Fig. 1B). And the increased LDH release in MSN-treated hepatocytes

was also shown in a dose-dependent manner (Fig. 1C). The *in vivo* effect of MSNs on livers was determined by tail intravenous injection at three different levels for three weeks. After the last injection, the mice were sacrificed and the serum samples were collected. Fig. 1D shows that the serum levels of LDH increased obviously at 25 mg kg⁻¹ and 50 mg kg⁻¹ dosage of MSNs. Blood biochemical parameters were also detected to reflect the hepatic functions. Serum ALT and AST levels increased significantly with MSN administration at 25 mg kg⁻¹ and 50 mg kg⁻¹, while no obvious increase was observed at 12.5 mg kg⁻¹ (Fig. 1E). In addition, representative images of MSN-induced hepatocellular damage are shown in Fig. S1.† These results indicated that MSNs induced obvious hepatotoxicity *in vitro* and *in vivo*.

3.2. MSNs activated NLRP3 inflammasomes and pyroptosis in hepatic cells and liver tissues

Generally, activated NLRP3 inflammasomes induce caspase-1 cleavage and IL-1 β maturation.³⁴ To identify whether the NLRP3 inflammasome was activated in MSN-treated hepatocytes, we detected the expression of NLRP3, IL-1 β and cleaved caspase-1. As shown in Fig. 2A, the levels of NLRP3, cleaved caspase-1 and IL-1 β increased in MSN-treated hepatocytes. And MSNs also increased the level of secreted IL-1 β in the cell culture medium (Fig. S2†). Hepatocyte immunofluorescence staining with the NLRP3 antibody showed that NLRP3 inflammasome activation was robust after MSN (120 μ g mL⁻¹) treatment *in vitro* (Fig. 2B). Moreover, caspase-1 activity was also augmented at the corresponding concentration points in MSN-treated hepatocytes (Fig. 2C). Based on the observation that caspase-1 was activated in MSN-treated hepatocytes, we then detected whether pyroptosis was triggered. Pyroptosis is dependent on caspase-1 activation and will cause pore formation on the cell membrane. Thus, PI and FAM-YVAD-FMK, a caspase-1-specific marker, were employed to examine pyropto-

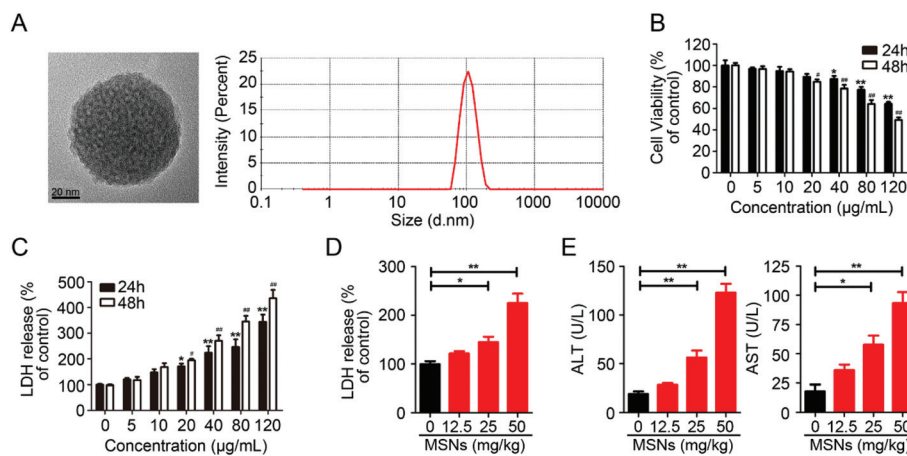


Fig. 1 Characterization and hepatotoxicity of MSNs. (A) The TEM image and diameter of the MSNs used in the present study. (B) Cytotoxicity of MSNs in hepatic cells. (C) The release of LDH in MSN-treated hepatocytes. (D) Serum levels of LDH after treatment with MSNs. (E) The ALT and AST level in the serum. Values in (B and C) are shown as mean \pm SD of three independent experiments. Values in (D and E) are shown as mean \pm SD and $n = 3$. (* and $^{\#}$ *p* < 0.05, ** and $^{##}$ *p* < 0.01 versus the relevant control).

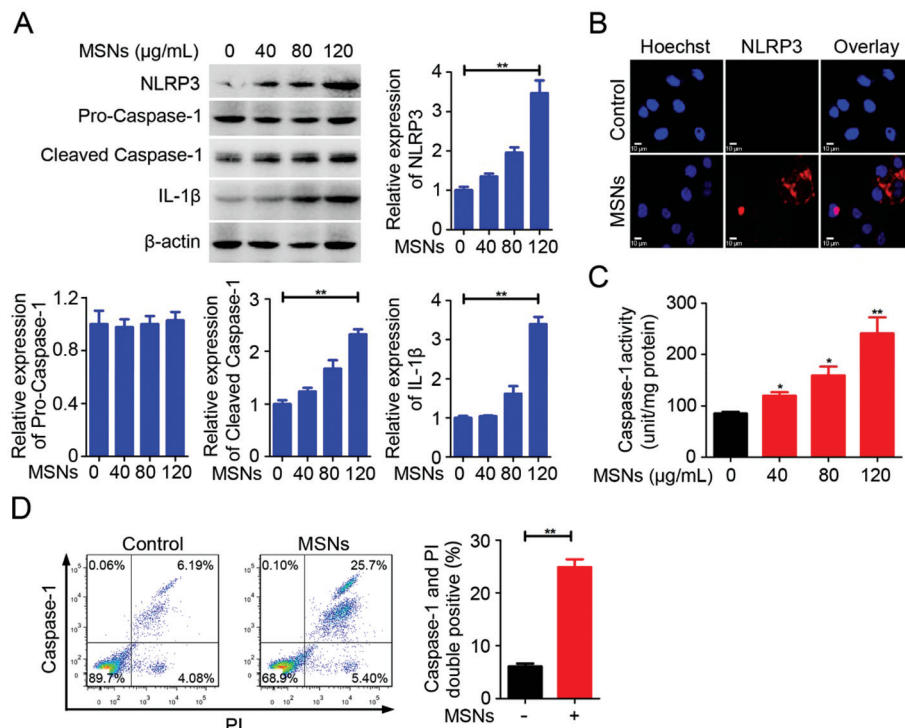


Fig. 2 MSNs activated NLRP3 inflammasomes and pyroptosis in hepatic cells. (A) The levels of NLRP3, IL-1 β , pro-caspase-1 and cleaved caspase-1 in hepatocytes were detected by western blot, and β -actin was used as a loading control. (B) Hepatocyte immunofluorescence staining with anti-NLRP3 antibody followed by MSN treatment. (C) Activity of caspase-1 following MSN treatment. (D) PI and FAM-YVAD-FMK were employed to examine MAN-induced hepatocyte pyroptosis via flow cytometry. Values are mean \pm SD and $n = 3$. * $p < 0.05$, ** $p < 0.01$.

sis *via* flow cytometry and the data indicated that the treatment with 120 μ g mL $^{-1}$ MSNs in hepatocytes showed a remarkable increase of pyroptosis (Fig. 2D).

Although NLRP3 inflammasomes and pyroptosis were proposed to be responsible for liver defense against pathogenic microorganism infection, their roles in MSN-mediated liver hepatotoxicity were still unclear. Therefore, we first measured NLRP3 inflammasomes in MSN-treated livers and found that the expression of NLRP3, IL-1 β , pro-caspase-1 and cleaved caspase-1 significantly increased (Fig. 3A and B). Liver immunofluorescence staining with the NLRP3 antibody showed that MSNs activated NLRP3 inflammasome *in vitro* (Fig. 3C). Serum IL-1 β and IL-18, and caspase-1 activity in liver homogenates were also significantly augmented (Fig. 3D and E). Notably, the co-staining of liver tissues with FAM-YVAD-FMK and PI displayed that MSN injection induced pyroptosis in the liver (Fig. 3F).

Collectively, the results demonstrated that MSNs triggered NLRP3 inflammasome activation, IL-1 β maturation and pyroptosis in hepatocytes and liver tissues.

3.3. NLRP3 inflammasome activation mediated MSN-elicited hepatocyte pyroptosis and liver injury

NLRP3 inflammasome activation induces pyroptosis *via* the cleavage and activation of caspase-1, and some reports also demonstrate that pyroptosis could be triggered by some other inflammasomes.³⁵ Thus, MCC950, a potent and selective

inhibitor of NLRP3, and NLRP3 knockdown were used to access the effects of NLRP3 inflammasomes in MSN-triggered hepatocyte pyroptosis and hepatotoxicity. As shown in Fig. 4A–C, the inhibition of NLRP3 by a pharmaceutical inhibitor or selective knockdown of NLRP3 abrogated MSN-elicited hepatocyte cytotoxicity and diminished MSN-activated NLRP3 inflammasomes in hepatic cells (Fig. 4D). In addition, a pharmaceutical inhibitor and siRNA successfully abrogated hepatocyte pyroptosis and caspase-1 activation caused by MSNs (Fig. 4E and F).

As shown in Fig. 5A and B, MSN-triggered NLRP3 inflammasome activation was abrogated by MCC950 as evidenced by the inhibition of the level of NLRP3, cleaved IL-1 β , pro-caspase-1 and cleaved caspase-1 in liver tissues. Then, the caspase-1 activity in liver homogenates, and the serum IL-1 β and serum IL-18 were determined, and we found that the administration of MCC950 attenuated the increased caspase-1 activity, serum IL-1 β and serum IL-18 caused by MSN treatment (Fig. 5C). To detect the function of NLRP3 inflammasome in MSN-mediated hepatotoxicity, serum ALT and AST were detected. As shown, abolishing NLRP3 inflammasome by MCC950 reversed the MSN-induced increase of ALT, AST and LDH to normal levels, indicating that the blockage of NLRP3 inflammasome significantly decreased MSN-elicited hepatotoxicity (Fig. 5D). As expected, the NLRP3 inhibitor notably decreased MSN-induced pyroptosis in liver tissues (Fig. 5E). In summary, these data indicated the MSN-elicited pyroptosis of

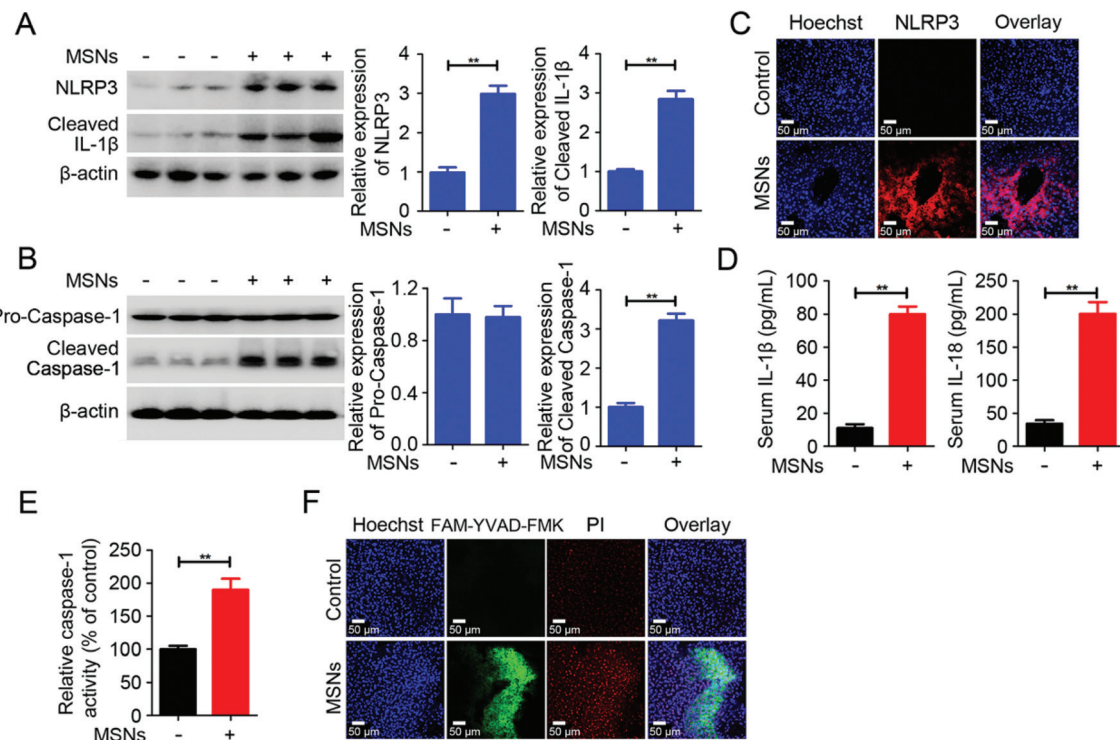


Fig. 3 NLRP3 inflammasome and pyroptosis were triggered by MSNs in the liver. (A and B) Immunoblotting was employed to detect the expression of NLRP3, IL-1 β , pro-caspase-1 and cleaved caspase-1 in the MSN-treated liver. (C) Liver immunofluorescence staining with anti-NLRP3 antibody followed by MSN treatment. (D) Serum IL-1 β and serum IL-18 were accessed. (E) Caspase-1 activity in liver homogenates. (F) Co-staining of liver tissues with FAM-YVAD-FMK and PI confirmed that MSNs-elicited pyroptosis. Values are mean \pm SD and $n = 3$. ** $p < 0.01$.

hepatic cells and liver injury through NLRP3 inflammasome activation.

3.4. NLRP3 deficiency alleviated MSN-elicited liver inflammation and hepatotoxicity

NLRP3^{-/-} mice were used to further identify whether NLRP3 inflammasome was the mediator in MSN-triggered liver inflammation and hepatotoxicity. Inconsistent with WT mice, MSN-triggered liver NLRP3 inflammasome activation almost entirely disappeared as evidenced by decreased cleaved caspase-1 and sightless IL-1 β in *NLRP3*^{-/-} mice (Fig. 6A). Correspondingly, in *NLRP3*^{-/-} mice, MSN-induced activation of caspase-1 in liver homogenates was completely abolished as well as the serum IL-1 β and IL-18 (Fig. 6B). As revealed by the levels of serum ALT, AST and LDH, MSN-induced hepatotoxicity could be prevented by NLRP3 knockout (Fig. 6C). These data suggested that NLRP3 was a pathogenic mediator in MSN-induced liver inflammation and hepatotoxicity.

3.5. Caspase-1 deficiency reversed MSN-induced liver inflammation and hepatotoxicity

Subsequently, the crucial roles of caspase-1 and caspase-1-dependent pyroptosis in MSN-induced liver inflammation and hepatotoxicity were investigated. In contrast to WT mice, caspase-1 double knockout (*Caspase-1*^{-/-}) mice had ameliorated liver inflammation as exhibited by the decreased

expression of NLRP3 and IL-1 β (Fig. 6D). Meanwhile, co-staining of FAM-YVAD-FMK and PI was employed to detect pyroptosis. We found that the deficiency of caspase-1 reduced the FAM-YVAD-FMK-positive cells induced by MSNs in the liver tissue (Fig. 6E). Furthermore, the effects of caspase-1 knockout in MSN-triggered liver injury were detected. As shown in Fig. 6F, MSN-induced serum ALT, AST and LDH upregulation were remarkably decreased in *Caspase-1*^{-/-} mice when compared with WT ones. Collectively, our results demonstrated that caspase-1 played a crucial role in MSN-induced hepatotoxicity, and the knockout of caspase-1 ameliorated MSN-elicited liver injury *via* the inhibition of NLRP3 inflammasome and pyroptosis.

3.6 Kupffer cells partially contributed to MSN-induced hepatotoxicity

As the specialized macrophages located in the liver, Kupffer cells played a critical role in the pathogenesis of liver inflammation. To detect whether Kupffer cells were involved in MSN-induced hepatotoxicity, mice were intravenously injected with clodronate liposomes to deplete Kupffer cells. As shown in Fig. S3A,† liver nonparenchymal cells were analyzed to confirm the efficient depletion of F4/80 $^{+}$ Kupffer cells (40.3% vs. 4.85%). Then, we found that the depletion of Kupffer cells could partially attenuate the MSN-induced increase of ALT, AST and LDH (Fig. S3B†). In addition, the depletion of Kupffer

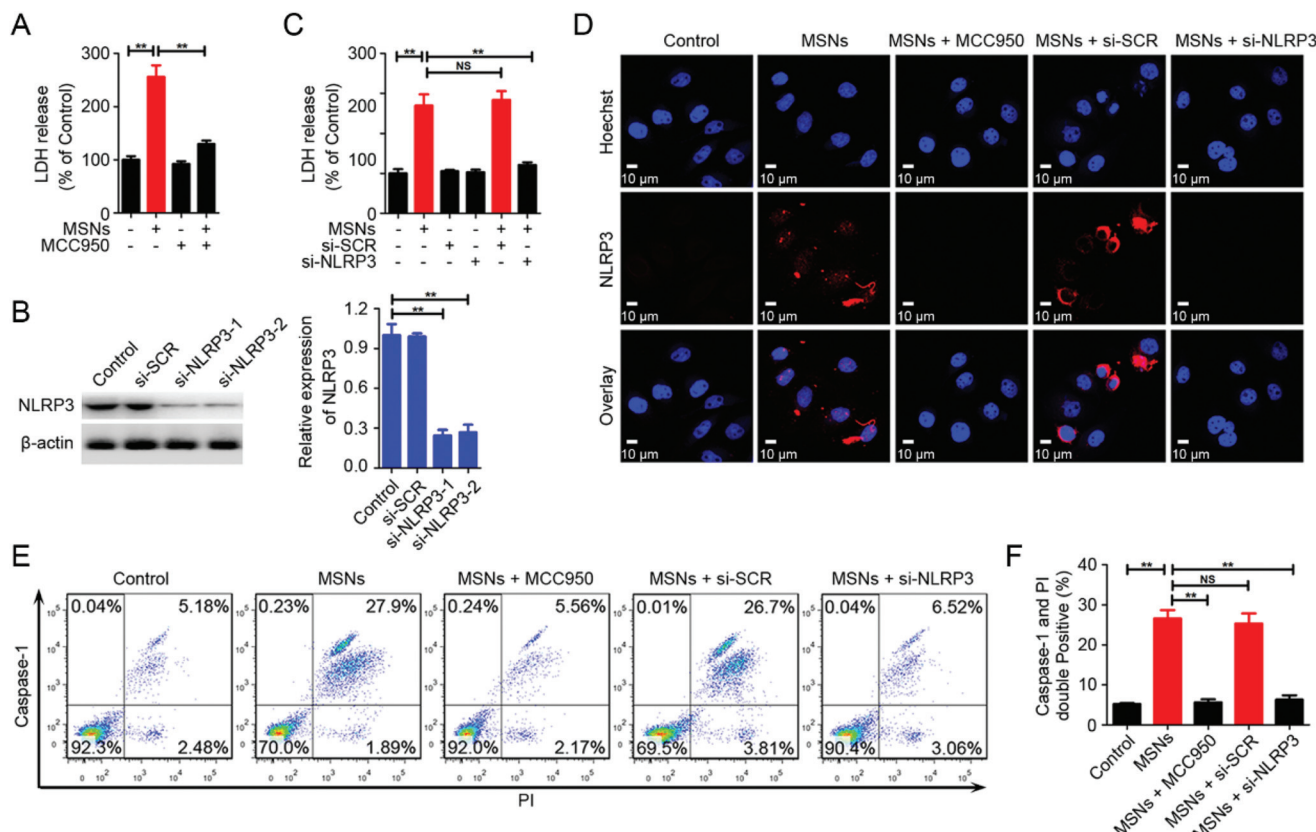


Fig. 4 Effect of activated NLRP3 inflammasomes in MSN-triggered hepatic cell pyroptosis. (A) The effects of NLRP3 inhibitor on MSN-induced LDH release in hepatic cells. (B and C) The effects of NLRP3 knockdown on MSN-induced LDH release in hepatic cells. Nonsilencing scrambled control (SCR) siRNA was used as a control. (D) NLRP3 inhibitor MCC950 and NLRP3 knockdown abrogated MSN-triggered NLRP3 inflammasome activation. (E) Effects of inhibitor and siRNA against NLRP3 on MSN-induced FAM-YVAD-FMK and PI double positive hepatocytes. (F) Statistical analysis of hepatocyte pyroptosis caused by MSNs *in vitro*. Values are shown as mean \pm SD and $n = 3$. ** $p < 0.01$; NS, no significance.

cells also partially reversed MSN-elicited NLRP3 inflammasome activation and pyroptosis of hepatic cells (Fig. S3C and S3D†). These data showed that Kupffer cells were involved in MSN-induced hepatotoxicity.

3.7. ROS was involved in MSN-activated NLRP3 and pyroptosis in liver

Research studies have shown that ROS production plays a critical role in the mechanism underlying NLRP3 inflammasome activation.³⁶ Therefore, to evaluate whether ROS was involved in MSN-activated NLRP3 inflammasomes and pyroptosis, we detected the level of total ROS in the primary hepatocytes by 2,7-dichlorofluorescein diacetate. As shown in Fig. 7A, the administration of MSNs significantly increased the intrahepatocellular ROS generation. Then MitoSox, a specific mitochondrial ROS probe, was employed to further demonstrate that the administration of MSNs increased ROS in liver tissues (Fig. S4A†). In general, ROS generation was accompanied by mitochondrial dysfunction. Thus, the JC-1 probe was applied to detect the mitochondrial membrane potential. JC-1 is a red aggregate at high membrane potential while a green monomer at low membrane potential. Our results showed that the MSN-

treated sample showed a green fluorescence, while the control sample showed a red fluorescence, indicating that MSN treatment induced mitochondrial dysfunction (Fig. S4B†). These data suggested that ROS participated in MSN-induced hepatotoxicity.

3.8 ROS scavenger obliterated MSN-caused hepatotoxicity via blocking NLRP3 activation

As shown in Fig. 7B, MSN-triggered ROS was markedly inhibited by the ROS scavenger NAC. Meanwhile, in the detection of the mitochondrial membrane potential, the NAC pretreated sample showed red fluorescence, implying that NAC restored mitochondrial membrane potential *via* the removal of ROS. Then, immunoblotting showed that NAC reduced the expression of NLRP3, IL-1 β , pro-caspase-1 and cleaved caspase-1 in the MSN-treated liver, indicating that MSN-induced ROS activated NLRP3 inflammasome (Fig. 7C). As we speculated, the ROS scavenger decreased caspase-1 activity and pyroptosis in the liver of MSN-treated mice (Fig. 7D and Fig. S5†). Levels of serum IL-1 β and serum IL-18 of MSN-treated mice were also downregulated by NAC (Fig. 7D). Furthermore, the levels of ALT, AST and LDH were also attenuated by NAC, indicating

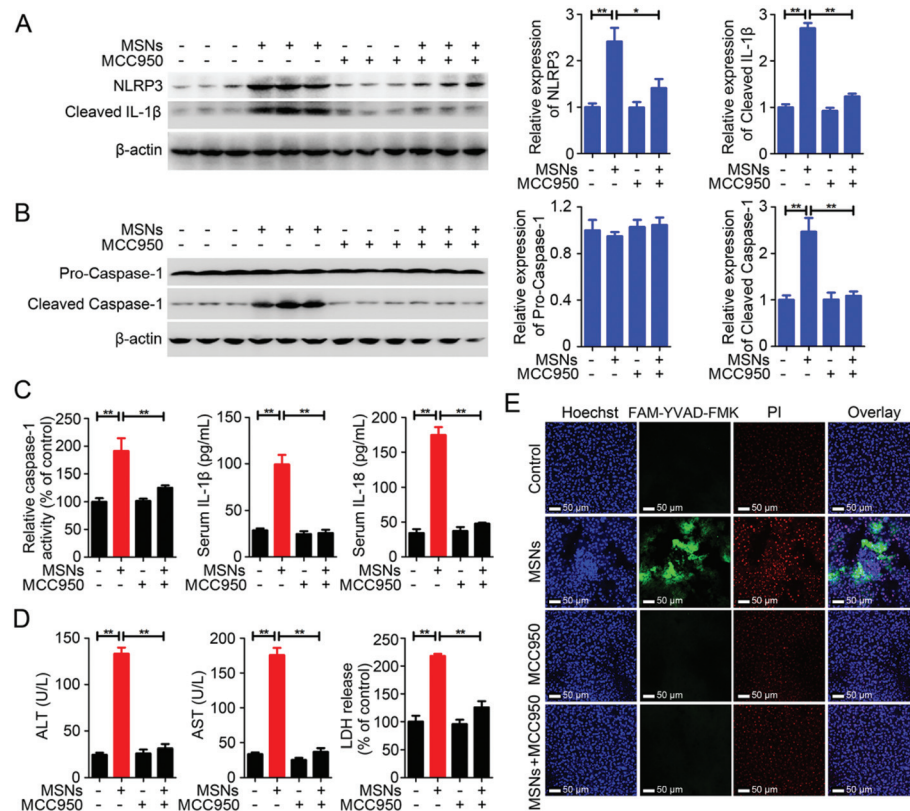


Fig. 5 The effect of activated NLRP3 inflammasomes in MSN-triggered pyroptosis and liver injury. (A and B) NLRP3 inhibitor MCC950 alleviated MSN-elicited increase of NLRP3, cleaved IL-1 β , pro-caspase-1 and cleaved caspase-1 *in vivo*. (C) Effects of MCC950 on the caspase-1 activity in liver homogenates, and serum IL-1 β and serum IL-18 after MSN administration. (D) Serum ALT, AST and LDH in the mice treated with MSNs and/or MCC950. (E) Co-staining of liver tissues with FAM-YVAD-FMK and PI displayed that MCC950 attenuates MSN injection-elicited pyroptosis. Values are shown as mean \pm SD and $n = 3$. * $p < 0.05$ and ** $p < 0.01$.

improved liver function (Fig. 7E). Taken together, these data indicated that ROS played a crucial role in MSN-activated NLRP3 inflammasomes and pyroptosis.

4. Discussion

The determination of biocompatibility associated with exposure to MSNs is of fundamental importance for the translation of these materials into biomedical applications, especially for the clinical applications.^{4,37} However, the assessment of toxicity caused by MSNs is still very poorly explored and understood. Although some initial reports have paid close attention to the toxicity of MSNs and the potential mechanisms, very little is known about MSN-induced hepatotoxicity.^{8,12,38} This study reported, for the first time, that MSNs activated NLRP3 inflammasomes, leading to undesirable toxicological effects in hepatocytes named caspase-1-dependent pyroptosis. Another principal finding of the present work was that the activation of NLRP3 inflammasomes mediated MSN-induced liver inflammation and hepatotoxicity. Notably pre-treatment with the NLRP3 inhibitor or knockout of NLRP3 and caspase-1 significantly rescued hepatocytes from MSN-induced

hepatotoxicity and reversed MSN-elicited liver inflammation. Furthermore, ROS generation as a main contributor to MSN-triggered NLRP3 activation was confirmed by the fact that the ROS scavenger could strikingly ameliorate the NLRP3 activation in hepatocytes. Herein, our results offered novel insights into MSN-triggered hepatotoxicity and elucidated the potential molecular mechanisms *in vitro* and *in vivo*, which could be exploited to develop a potential approach to eliminate the side effect of MSNs and facilitate the biomedical applications.

Several literature reports have shown that MSNs could reduce cell viability in various cell types, including monocyte-derived dendritic cells, human melanoma A375 cells, alveolar macrophages and colon carcinoma cell line Caco-2.^{8,10,38,39} Consistent with these research studies, our work indicated that MSNs induced cell growth inhibition and cell death in hepatocytes. Some studies reported that MSN treatment did not decrease the cell viability *in vitro*.^{40,41} The difference might be caused by the discrepancy in experimental systems, including cell types, interaction time, dose, particle shape, particle size and surface chemistry, all of which could directly affect the cytotoxicity of MSNs.⁴² Research has investigated the effects of the size of silica particle and showed that the nano-

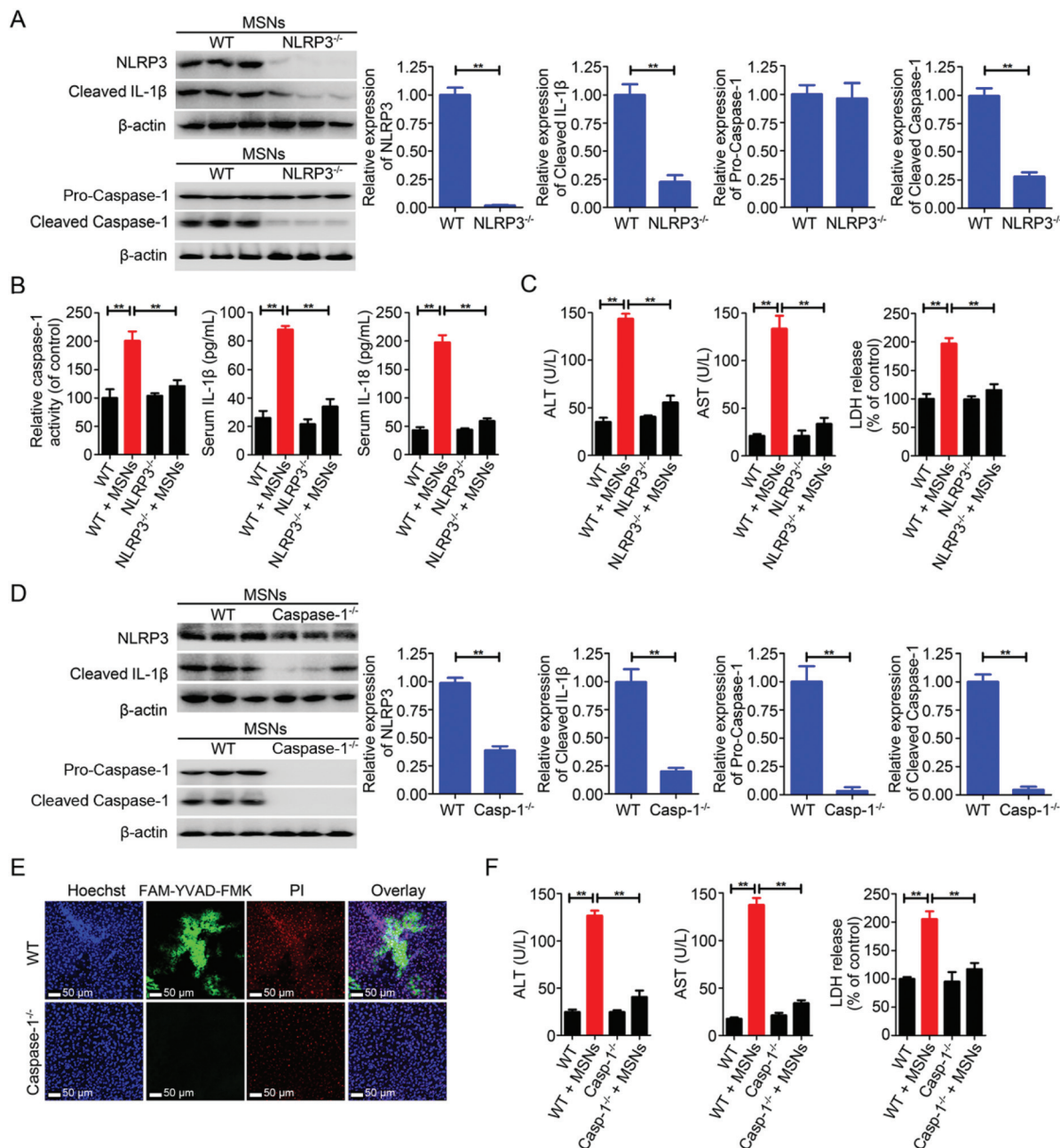


Fig. 6 NLRP3 deficiency and caspase-1 deficiency reversed MSN-elicited liver inflammation and hepatotoxicity. (A) NLRP3 knockout abolished the upregulation of cleaved caspase-1 and IL-1 β triggered by MSNs in the liver. (B) The caspase-1 activity in liver homogenates, serum IL-1 β and serum IL-18 after MSN administration in NLRP3 deficiency mice. (C) Serum ALT, AST and LDH following MSN administration in NLRP3 knockout mice. (D) Caspase-1 knockout suppressed the upregulation of NLRP3 and IL-1 β caused by MSNs. (E) Caspase-1 deficiency abolished MSN-induced pyroptosis in the liver. (F) Serum ALT, AST and LDH following MSN administration in caspase-1 knockout mice. Values are shown as mean \pm SD and $n = 3$. ** $p < 0.01$.

particle with the size above 50 nm could induce significant cytotoxicity, and the pro-inflammatory cytokines IL-1 β and TNF- α could also be induced by the silica nanoparticle with diameters of 50 or 100 nm.⁴³ Similarly, our MSNs, with the mean size of 109.2 nm, could trigger inflammasome and pyroptosis in hepatocytes. Caspase-3/7 was demonstrated to be involved in MSN-induced cytotoxicity in several cell types and

silicon nanoparticles could trigger NO production and IL-6 secretion.^{8,39} In this study, MSNs were confirmed to activate NLRP3 inflammasomes in hepatic cells for the first time. When NLRP3 inflammasomes are activated, the PYD domain mediates the form of the NLRP3 inflammasome complex, leading to caspase-1 activation and caspase-1-dependent cell death.^{44,45} Our results further revealed that NLRP3 inflamma-

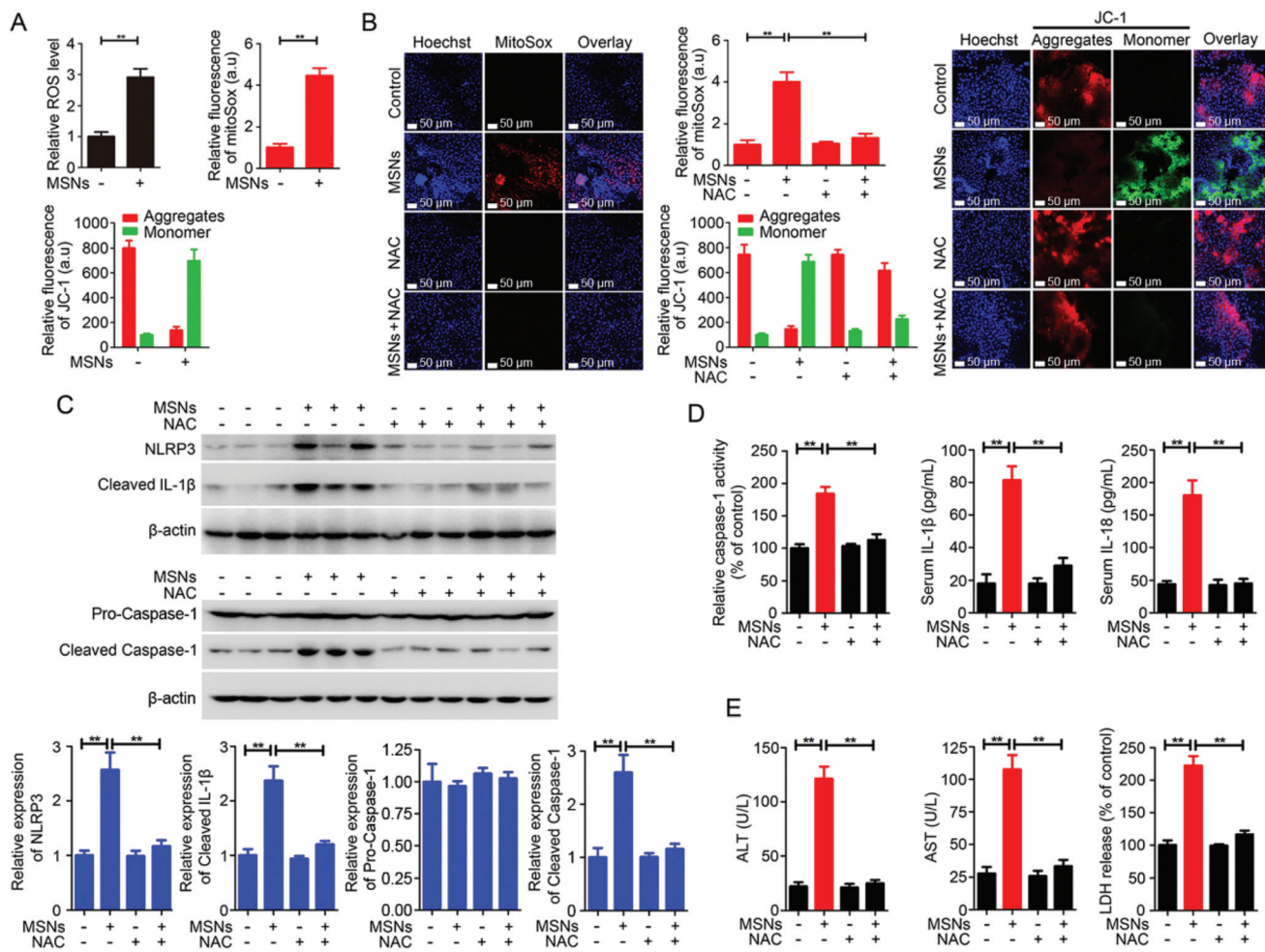


Fig. 7 MSN-triggered NLRP3 activation and pyroptosis were mediated by ROS in the liver. (A) ROS and mitochondrial membrane potential in the liver after MSN treatment. (B) Inhibition of NAC on MSN-elicited production of ROS and dysfunction of mitochondrial membrane potential. (C) ROS scavenger abolished the increased expression of NLRP3, cleaved IL-1 β , pro-caspase-1 and cleaved caspase-1 caused by MSNs in the liver. (D) The caspase-1 activity in liver homogenates, and serum IL-1 β and serum IL-18 after MSN administration in NAC-pretreated mice. (E) The effects of NAC on ALT, AST and LDH in the liver after MSN administration. Values are mean \pm SD and $n = 3$. ** $p < 0.01$.

some mediated MSN-elicited hepatocyte pyroptosis. Previous reports have showed that NLRP3 inflammasome was activated in hepatic parenchymal cells under various pathogenic stimuli and caused hepatocyte pyroptosis.²¹ Therefore, we reasonably proposed that the activated NLRP3 inflammasomes and the resulting pyroptosis are novel mechanisms underlying MSN-elicited hepatotoxicity.

Although *in vitro* evaluations could provide profound insights into MSN-elicited NLRP3 inflammasome and pyroptosis at molecular and subcellular levels, *in vivo* investigations on the hepatotoxicity of MSNs are more important for further facilitating the potential biomedical and clinical applications. Silica nanoparticles have been indicated to trigger sustained inflammation and dysfunction in the lung.⁴⁶ In the liver, it was reported that a single dose of MSNs showed low single dose toxicity, while various effects were observed after multiple doses of MSN administration, such as oxidative stress, morphological impairment, degenerative necrosis of hepatocytes

and pro-inflammatory responses.^{47,48} These results are in accordance with our study which showed that MSN treatment triggered liver inflammation and hepatotoxicity. However, mechanisms of MSN-activated hepatotoxicity have not been clarified. Given the critical roles of NLRP3 in promoting inflammation, the NLRP3 inflammasome was further assessed in MSN-elicited hepatotoxicity. Consistent with the *in vitro* results, NLRP3 inflammasome was activated *in vivo* by MSNs, and plays a critical role in mediating liver inflammation and hepatotoxicity. And a previous study reported that pyroptosis contributed to QD-induced cytotoxicity.²⁹ So, based on the caspase-1 knockout mice, we confirmed the role of pyroptosis in MSN-induced hepatotoxicity. To the best of our knowledge, it is the first *in vivo* demonstration of the mechanisms involved in MSN-induced hepatotoxicity.

NLRP3 inflammasome could be activated by varieties of sensors, such as potassium ion efflux, the release of lysosomal cathepsins and the release of mitochondrion DNA. And sub-

sequent studies demonstrated that mitochondria-derived ROS was considered as a major activator in NLRP3 inflammasome formation.⁴⁹ Importantly, crystalline silica nanoparticles cause ROS formation *in vitro* which compromises cellular viability. Heikkilä *T et al.* reported that MSNs induced ROS formation at high concentrations in oral drug formulations.⁸ Silicon-based nanoparticles could enter mitochondria and cause mitochondrial swelling which contributed to ROS generation, and ROS generation could activate the NLRP3 inflammasome through the NF- κ B pathway.^{27,50} In the present study, the data indicated that MSNs resulted in hepatocyte ROS generation after MSN administration, accompanied by mitochondrial dysfunction. Furthermore, ROS was confirmed to mediate MSN-activated NLRP3 and pyroptosis. Notably, serum LDH, ALT, and AST in MSN-treated mice were also attenuated by the ROS scavenger, indicating the improved liver functions. Our results provided novel insights into MSN-triggered hepatotoxicity that MSNs induced liver inflammation and hepatocyte pyroptosis through NLRP3 inflammasome activation, which was caused by MSN-induced ROS production, indicating that combined with the inhibitors targeting NLRP3 inflammasome, pyroptosis or ROS could improve the biosafety of MSNs.

5. Conclusion

In summary, this study focused on elucidating the molecular mechanism of hepatic toxicity induced by MSNs *in vitro* and *in vivo*. Our results demonstrated that MSNs elicited liver inflammation, hepatic cell pyroptosis and hepatotoxicity. The hepatotoxicity was dependent on activated NLRP3 inflammasomes which was due to ROS production after treatment with MSNs. These results provided novel insights into MSN-elicited hepatotoxicity, indicating that NLRP3 inflammasome, pyroptosis and ROS are potent targets for improving the biocompatibility and reducing the potential toxicity of MSNs. Further research to evaluate the relationship between hepatotoxicity and sizes or surface chemical modification of MSNs *in vivo* is needed, which could ultimately be used to avoid the side effect of MSNs in potential biomedical applications.

Conflicts of interest

All the authors have no conflicts of interest to declare.

Acknowledgements

This work was supported by the grants of the National Key Basic Research Program of China (2015CB931800), the National Natural Science Foundation of China (81573332 and 81773620), and the Special Research Foundation of State Key Laboratory of Medical Genomics and Collaborative Innovation Center of Systems Biomedicine. We are grateful to Dr Warren Strober for providing NLRP3 knockout mice.

References

- 1 A. Mukerjee, A. P. Ranjan and J. K. Vishwanatha, *Curr. Med. Chem.*, 2012, **19**, 3714–3721.
- 2 J. Fan, Y. Sun, S. Wang, Y. Li, X. Zeng, Z. Cao, P. Yang, P. Song, Z. Wang, Z. Xian, H. Gao, Q. Chen, D. Cui and D. Ju, *Biomaterials*, 2016, **78**, 102–114.
- 3 S. E. Kim, L. Zhang, K. Ma, M. Riegman, F. Chen, I. Ingold, M. Conrad, M. Z. Turker, M. Gao, X. Jiang, S. Monette, M. Pauliah, M. Gonen, P. Zanzonico, T. Quinn, U. Wiesner, M. S. Bradbury and M. Overholtzer, *Nat. Nanotechnol.*, 2016, **11**, 977–985.
- 4 X. Du, X. Li, L. Xiong, X. Zhang, F. Kleitz and S. Z. Qiao, *Biomaterials*, 2016, **91**, 90–127.
- 5 J. H. Park, L. Gu, G. von Maltzahn, E. Ruoslahti, S. N. Bhatia and M. J. Sailor, *Nat. Mater.*, 2009, **8**, 331–336.
- 6 Z. Zou, X. He, D. He, K. Wang, Z. Qing, X. Yang, L. Wen, J. Xiong, L. Li and L. Cai, *Biomaterials*, 2015, **58**, 35–45.
- 7 C. M. Sayes, K. L. Reed, K. P. Glover, K. A. Swain, M. L. Ostraat, E. M. Donner and D. B. Warheit, *Inhalation Toxicol.*, 2010, **22**, 348–354.
- 8 T. Heikkilä, H. A. Santos, N. Kumar, D. Y. Murzin, J. Salonen, T. Laaksonen, L. Peltonen, J. Hirvonen and V. P. Lehto, *J. Pharm. Biopharm.*, 2010, **74**, 483–494.
- 9 R. Diab, N. Canilho, I. A. Pavel, F. B. Haffner, M. Girardon and A. Pasc, *Adv. Colloid Interface Sci.*, 2017, **249**, 346–362.
- 10 Y. Song, Y. Li, Q. Xu and Z. Liu, *Int. J. Nanomed.*, 2017, **12**, 87–110.
- 11 C. Fu, T. Liu, L. Li, H. Liu, D. Chen and F. Tang, *Biomaterials*, 2013, **34**, 2565–2575.
- 12 T. Liu, L. Li, X. Teng, X. Huang, H. Liu, D. Chen, J. Ren, J. He and F. Tang, *Biomaterials*, 2011, **32**, 1657–1668.
- 13 E. B. Ehlerding, F. Chen and W. Cai, *Adv. Sci.*, 2016, **3**, 1500223.
- 14 J. G. Croissant, Y. Fatieiev and N. M. Khashab, *Adv. Mater.*, 2017, **29**, 1604634.
- 15 C. E. Ashley, E. C. Carnes, G. K. Phillips, D. Padilla, P. N. Durfee, P. A. Brown, T. N. Hanna, J. Liu, B. Phillips, M. B. Carter, N. J. Carroll, X. Jiang, D. R. Dunphy, C. L. Willman, D. N. Petsev, D. G. Evans, A. N. Parikh, B. Chackerian, W. Wharton, D. S. Peabody and C. J. Brinker, *Nat. Mater.*, 2011, **10**, 389–397.
- 16 N. Rawat, Sandhya, K. Subaharan, M. Eswaramoorthy and G. Kaul, *Toxicol. Ind. Health*, 2017, **33**, 182–192.
- 17 G. Szabo and T. Csak, *J. Hepatol.*, 2012, **57**, 642–654.
- 18 S. M. Man, R. Karki, M. Sasai, D. E. Place, S. Kesavardhana, J. Temirov, S. Frase, Q. Zhu, R. K. S. Malireddi, T. Kuriakose, J. L. Peters, G. Neale, S. A. Brown, M. Yamamoto and T. D. Kanneganti, *Cell*, 2016, **167**, 382–396.
- 19 K. Schroder and J. Tschoop, *Cell*, 2010, **140**, 821–832.
- 20 A. Lu, V. G. Magupalli, J. Ruan, Q. Yin, M. K. Atianand, M. R. Vos, G. F. Schroder, K. A. Fitzgerald, H. Wu and E. H. Egelman, *Cell*, 2014, **156**, 1193–1206.
- 21 M. Lamkanfi and V. M. Dixit, *Cell*, 2014, **157**, 1013–1022.

- 22 W. Chen, X. Zhang, J. Fan, W. Zai, J. Luan, Y. Li, S. Wang, Q. Chen, Y. Wang, Y. Liang and D. Ju, *Theranostics*, 2017, **7**, 4135–4148.
- 23 R. Zhou, A. S. Yazdi, P. Menu and J. Tschopp, *Nature*, 2011, **469**, 221–225.
- 24 T. Strowig, J. Henao-Mejia, E. Elinav and R. Flavell, *Nature*, 2012, **481**, 278–286.
- 25 B. Ke, W. Shen, X. Fang and Q. Wu, *J. Cell. Mol. Med.*, 2018, **22**, 16–24.
- 26 E. Ozaki, M. Campbell and S. L. Doyle, *J. Inflammation Res.*, 2015, **8**, 15–27.
- 27 B. Sun, X. Wang, Z. Ji, M. Wang, Y. P. Liao, C. H. Chang, R. Li, H. Zhang, A. E. Nel and T. Xia, *Small*, 2015, **11**, 2087–2097.
- 28 Y. B. Li, S. F. Wang, J. J. Fan, X. S. Zhang, X. L. Qian, X. Y. Zhang, J. Y. Luan, P. Song, Z. Y. Wang, Q. C. Chen and D. W. Ju, *ACS Biomater. Sci. Eng.*, 2017, **3**, 843–853.
- 29 Y. Lu, S. Xu, H. Chen, M. He, Y. Deng, Z. Cao, H. Pi, C. Chen, M. Li, Q. Ma, P. Gao, Y. Ji, L. Zhang, Z. Yu and Z. Zhou, *Biomaterials*, 2016, **90**, 27–39.
- 30 D. Shen, J. Yang, X. Li, L. Zhou, R. Zhang, W. Li, L. Chen, R. Wang, F. Zhang and D. Zhao, *Nano Lett.*, 2014, **14**, 923–932.
- 31 G. Meng, F. Zhang, I. Fuss, A. Kitani and W. Strober, *Immunity*, 2009, **30**, 875–887.
- 32 K. Mao, S. Chen, M. Chen, Y. Ma, W. Yan, H. Bo, Z. He, Y. Zeng, Y. Hu, S. Sun, J. Li, X. Wu, X. Wang, W. Strober, C. Chen, G. Meng and B. Sun, *Cell Res.*, 2013, **23**, 201–212.
- 33 X. Zhang, J. Fan, S. Wang, Y. Li, Y. Wang, S. Li, J. Luan, Z. Wang, P. Song, Q. Chen, W. Tian and D. Ju, *Cancer Immunol. Res.*, 2017, **5**, 363–375.
- 34 J. Yu, H. Nagasu, T. Murakami, H. Hoang, L. Broderick, H. M. Hoffman and T. Horng, *Proc. Natl. Acad. Sci. U. S. A.*, 2014, **111**, 15514–15519.
- 35 D. M. Cerqueira, M. S. Pereira, A. L. Silva, L. D. Cunha and D. S. Zamboni, *J. Immunol.*, 2015, **195**, 2303–2311.
- 36 S. Han, W. Cai, X. Yang, Y. Jia, Z. Zheng, H. Wang, J. Li, Y. Li, J. Gao, L. Fan and D. Hu, *Mediators Inflammation*, 2015, **2015**, 720457.
- 37 M. Zhang, C. Xu, L. Wen, M. K. Han, B. Xiao, J. Zhou, Y. Zhang, Z. Zhang, E. Viennois and D. Merlin, *Cancer Res.*, 2016, **76**, 7208–7218.
- 38 X. Huang, X. Teng, D. Chen, F. Tang and J. He, *Biomaterials*, 2010, **31**, 438–448.
- 39 L. Di Cristo, D. Movia, M. G. Bianchi, M. Allegrini, B. M. Mohamed, A. P. Bell, C. Moore, S. Pinelli, K. Rasmussen, J. Riego-Sintes, A. Prina-Mello, O. Bussolati and E. Bergamaschi, *Toxicol. Sci.*, 2016, **150**, 40–53.
- 40 M. Wu, Q. Meng, Y. Chen, Y. Du, L. Zhang, Y. Li, L. Zhang and J. Shi, *Adv. Mater.*, 2015, **27**, 215–222.
- 41 X. Chen, H. Sun, J. Hu, X. Han, H. Liu and Y. Hu, *Biointerfaces*, 2017, **152**, 77–84.
- 42 A. Albanese, P. S. Tang and W. C. Chan, *Annu. Rev. Biomed. Eng.*, 2012, **14**, 1–16.
- 43 N. Nishijima, T. Hirai, K. Misato, M. Aoyama, E. Kuroda, K. J. Ishii, K. Higashisaka, Y. Yoshioka and Y. Tsutsumi, *Front. Immunol.*, 2017, **8**, 379.
- 44 A. S. Yazdi, G. Guarda, N. Riteau, S. K. Drexler, A. Tardivel, I. Couillin and J. Tschopp, *Proc. Natl. Acad. Sci. U. S. A.*, 2010, **107**, 19449–19454.
- 45 A. Wree, A. Eguchi, M. D. McGeough, C. A. Pena, C. D. Johnson, A. Canbay, H. M. Hoffman and A. E. Feldstein, *Hepatology*, 2014, **59**, 898–910.
- 46 R. F. Hamilton Jr., S. A. Thakur and A. Holian, *Free Radicals Biol. Med.*, 2008, **44**, 1246–1258.
- 47 T. Liu, L. Li, C. Fu, H. Liu, D. Chen and F. Tang, *Biomaterials*, 2012, **33**, 2399–2407.
- 48 D. Rees and J. Murray, *Int. J. Tuberc. Lung Dis.*, 2007, **11**, 474–484.
- 49 J. Tschopp and K. Schroder, *Nat. Rev. Immunol.*, 2010, **10**, 210–215.
- 50 C. Guo, J. Wang, L. Jing, R. Ma, X. Liu, L. Gao, L. Cao, J. Duan, X. Zhou, Y. Li and Z. Sun, *Environ. Pollut.*, 2018, **236**, 926–936.